Sensors & Diagnostics

PAPER

View Article Online
View Journal

Cite this: DOI: 10.1039/d5sd00218d

A multilayer fluorogenic material for the ultrasensitive detection of TATP in air, suitable for implementation on a mechanized semi-autonomous robotic platform

Irene Abajo-Cuadrado,[a] Andrea Revilla-Cuesta,[a] Ricardo Fernández-Ordóñez,[a] J. Rafael Santana-Tejada,[a] Yeray Moreno-Macías,[a] Cristian Almeida-Estévez,[a] Carla Hernando-Muñoz,[a] José García-Calvo, †[a] Manuel Avella [b] and Tomás Torroba *[a]

Received 3rd December 2025,
Accepted 18th March 2026

DOI: 10.1039/d5sd00218d

rsc.li/sensors

We describe a multilayer fluorogenic material, composed of a fluorescent probe supported on silica, polydimethylsiloxane and glass slides, that is implemented on a mechanized device for semi-autonomous measurements of airborne triacetone triperoxide (TATP) in operational spaces. By using a UV LED and a commercial micro-fluorometer as the measuring block, a mini-PC and a Wi-Fi card as the control block, all integrated in a mobile robotic platform, and a mobile phone as the receiver, we have constructed the first semiautonomous airborne TATP detection system useful for scanning the presence of IEDs in routine environments. It worked by exposing a sensing stick to the air flow in a room and sending the remote measurements to a mobile phone app. The presence of TATP is subsequently detected by the difference in the fluorescence signal from the initial and final measurements. The system can help combat the threat of improvised explosive devices (IEDs) composed of TATP.

Introduction

Improvised explosive devices (IEDs) pose some risk in the normal life of everyone. They were initially used in war scenarios but then quickly moved to the terrorist attacks in western countries and now they are an everyday risk.[1] The social and economic consequences of terrorism have been substantial by causing large direct and indirect costs, which may range from the loss of human lives and the destruction of assets to reduced economic growth and life satisfaction. In 2024, 58 terrorist attacks were recorded in the European Union, of which 34 were completed, which marked a significant increase from 2023. Burning, bombing, IEDs and improvised incendiary devices (IIDs) were employed in most of the attacks.[2] Between the many known explosives that can be used to construct IEDs, one of them surpasses the rest in the easy availability and use in IED terrorist attacks; it is constituted by triacetone triperoxide (TATP), a white powder that is prepared at home from simple precursors that can be found at the supermarket.[3] It was used, as a well-known example, at the March 22, 2016 airport bombing in Belgium.[4] The fact that TATP could be prepared on site during a long flight is the reason that liquids are forbidden in the airplane cabin of commercial flights.[5] Thus, our everyday life is threatened by this substance. Other substances such as hexamethylene triperoxide triamine (HMTD), albeit of terrorists' interest, are less used.[6] TATP is a volatile compound but has no odour, but dogs can be trained to detect it,[7] albeit they are most commonly trained for the detection of classic nitrated explosives such as trinitrotoluene (TNT), a common explosive that is also routinely checked for by fluorescence swab at airport checkpoints.[8,9] But there is no commercial system for the detection of TATP, despite its enormous importance in everyday life.[10,11] While the science community has produced several hundreds of chemical probes through the years, possibly all of them work well in the laboratory but not many are suitable for detection of analytes in real environments under common life conditions. As a main subject of research, we have been working in chemical sensors for especially important analytes, such as toxins,[12] nitrated[13] or peroxide[14] explosives, and chemical weapons.[15] Methods of detection in air are less common but most necessary for real life applications.[16–25] For practical

[a] Department of Chemistry, Faculty of Science, University of Burgos, 09001 Burgos, Spain. E-mail: ttorroba@ubu.es
[b] Electron Microscopy Lab, IMDEA Materials Institute, Eric Kandel, 2, Tecnogetafe, 28906 Getafe (Madrid), Spain
† Permanent address: Department of Organic Chemistry, Faculty of Science, Autonomous University of Madrid, 28049 Madrid, Spain.

applications, some problems have to be resolved such as sampling in public spaces[26,27] or automatization.[28,29] Directed oxidation of surfaces by external agents with a subsequent change in spectroscopic properties[30,31] constitutes a useful approach for the design of new sensor materials in the gas phase. The easy sublimation of TATP should permit its detection from hidden sources of the material in the gas phase. By the controlled detection of the oxidation of a fluorescent dye on the surface of silica nanoparticles, we have previously described a functional test unit for the detection of TATP, the most common component in IEDs.[32] The material was able to detect traces of TATP in air with an extremely low limit of detection (LOD = 13.3 ng L^{-1} measured in a microfluidic device), in environments suitable for use under normal living conditions, such as a regular office. It worked by an increase of the fluorescence signal in the presence of TATP traces, therefore taking measurements before and after the presence of the suspected TATP in the air gave a quantitative detection of the presence and the amount of the substance. We envisioned that by using such material in a mechanical device, IEDs concealed in confined public spaces could be detected, but technical improvements in the use need to be accomplished. Building upon the concept, we have now developed a standardized methodology to support the material on Sylgard 184, a standard polydimethylsiloxane (PDMS), on glass slides of a specific shape and thickness, so it can be used in a mechanized device for autonomous measurements. By using a UV LED and a commercial microfluorometer (Hamamatsu) as the measuring block, a mini-PC and a Wi-Fi card as the control block, all integrated in a controlled or semiautonomous platform (a home-made terrestrial robot), and a mobile phone as the receiver, we have constructed the first semiautonomous TATP detector system that can be used for standard scanning of IEDs in routine environments or terrorist scenarios, where it is suspected that TATP can be present. The new system works by exposing a previously background-measured multilayer detection stick to the air flow in a room or any part of a closed building, moving the stick to take measurements at fixed time periods on a fluorometer assembled in the system, and sending the measurements to a mobile phone by an Excel application and a Wi-Fi communication protocol. The presence of TATP is subsequently detected by the difference in the fluorescence signal from the initial and final measurements taken along the protocol. The system is suitable for many improvements and applications, for example, the sticks are wearable so they can be part of the police or soldier's equipment in search of IEDs and the semiautonomous platform can be used as the mobile measurement detection, therefore multiplying the possibilities of IED detection in the field. The system has been improved for its use in operational scenarios, on the way to commercialization for standard use in confined public spaces such as an airplane cargo hold or a stadium storage area where the threat of IEDs including TATP is suspected. The device will improve the safety of citizens in the fight against terrorism as a threat so the IEDs used in terrorist attacks can be detected before they cause any harm. The results of the research are presented here.

Results and discussion

Preparation of material

The material used for TATP detection consisted of a glass on which a layer of Sylgard-184 and a layer of silica nanoparticles were deposited, then the active dye [(piperidin-4-yl)-4-[2-(4-Boc-piperazin-1-yl)pyrimidin-5-yl]naphthalene-1,8-dicarboxylmonoimide][32] (ACTD) was adsorbed on the nanoparticles, so the multilayer material was ready for TATP detection (Fig. 1). First, microscopy slides (Deltalab) were cut into approximately 38 × 10 mm size strips with a diamond tip and cleaned with ethanol. The strips are then placed in the chuck at the center of a spin coating machine chamber (Laurell), held under vacuum and the chamber under compressed/clean dry air (CDA) at 4–5 bar, from a Sicolab compressor (Fig. 1, a)). A layer of Sylgard-184 was deposited on their surface by using a static procedure, in which Sylgard-184 (where the polymer was in a 1 : 0.1 ratio with the crosslinking agent) was deposited on a non-rotating substrate with a syringe and then rotated at a spreading step of 500 rpm for 2 seconds, casting step of 1500 rpm for 10 seconds, and final step of 3000 rpm for 30 seconds (Fig. 1, b)). Then, a layer of silica nanoparticles (Aldrich, nanopowder, 10–20 nm particle size, 99.5% trace metals basis) (Fig. 1, c)) was deposited on Sylgard-184 and the system was cured in an oven for 2 hours at 70 °C (Fig. 1, d)). After Sylgard-184 was cured, the excess silica nanoparticles that were not attached to the adhesive layer were removed. Then, 0.12 mg of the active dye (ACTD),[32] dissolved in 8 ml of chloroform, were poured into a glass reaction vessel (Fig. 1, e)), a silica covered strip was placed and the reaction vessel was covered with Parafilm and stirred by an orbital shaker under a stream of nitrogen for 20 minutes, until evaporation of the solvent and adsorption of the ACTD on the silica nanoparticles (Fig. 1, f)). Deposition of ACTD on silica nanoparticles was followed by structural and elemental TEM images of the ACTD@SiO_2 nanoparticles, as well as high resolution TEM images and elemental composition by EDX (Fig. 2).

In-the-office-room measurements of airborne TATP

The material was checked for its performance for out-of-the-laboratory portable measurements of airborne TATP in a typical (15 m^2) study room with the shape and dimensions shown in Fig. 3. The experiments were standardized to 5 mg of TATP, which was placed at 30 cm from a source of a continuous stream of clean air (100 cm^3 min^{-1}, 0.8 cm internal diameter), and evaporated by the air stream on the way to the sensing strips, which where exposed to TATP vapor for 30 minutes, maintaining the temperature at 25 °C, at increasing distances from the TATP sample (10, 25, 50, 75, 100, 150, 200 and 300 cm). The emission spectra of the glass

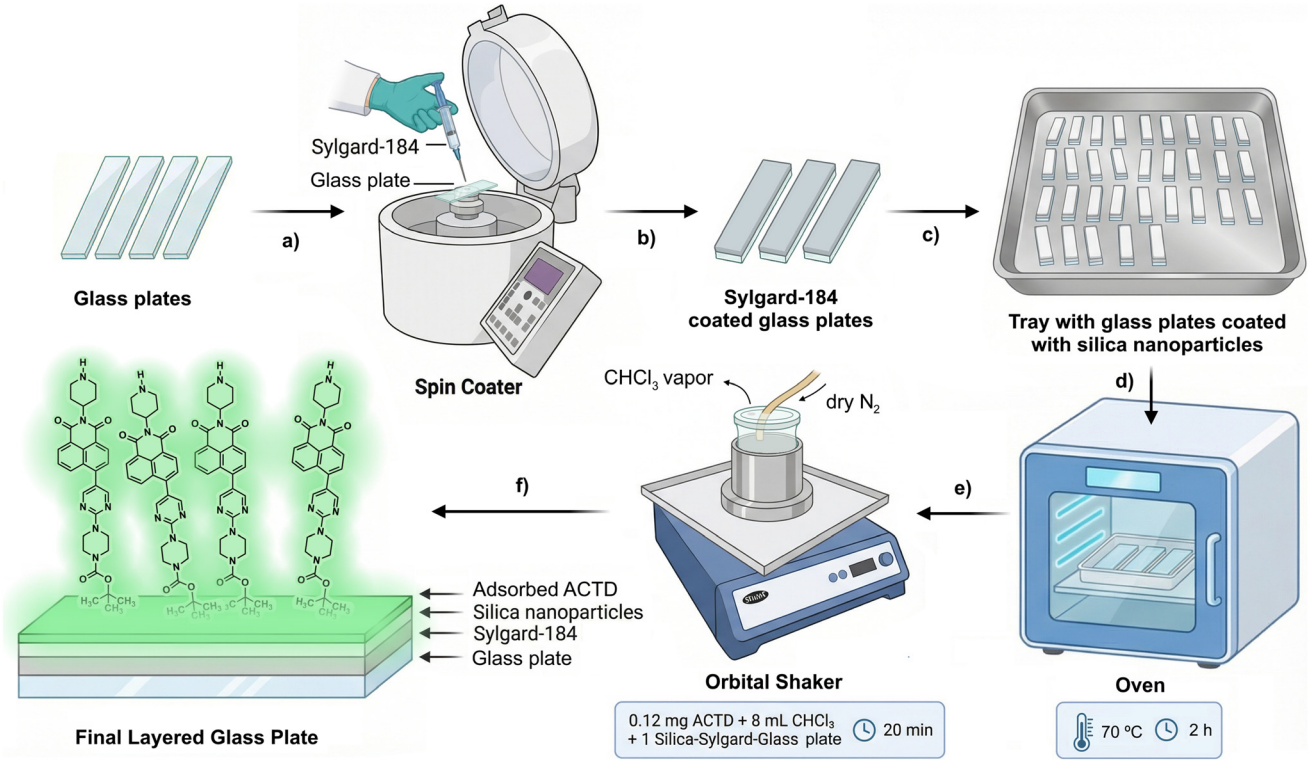

Fig. 1 Materials used in the deposition of the Sylgard-184 and silica nanoparticles layers: cut glass plates are used for deposition of (a) Sylgard-184 by syringe and spin-coating, (b) aligning, (c) depositing silica nanoparticles, (d) curing in oven and (e) adsorption of the ACTD on the multilayer plates to get (f) the final multilayer sensing strips.

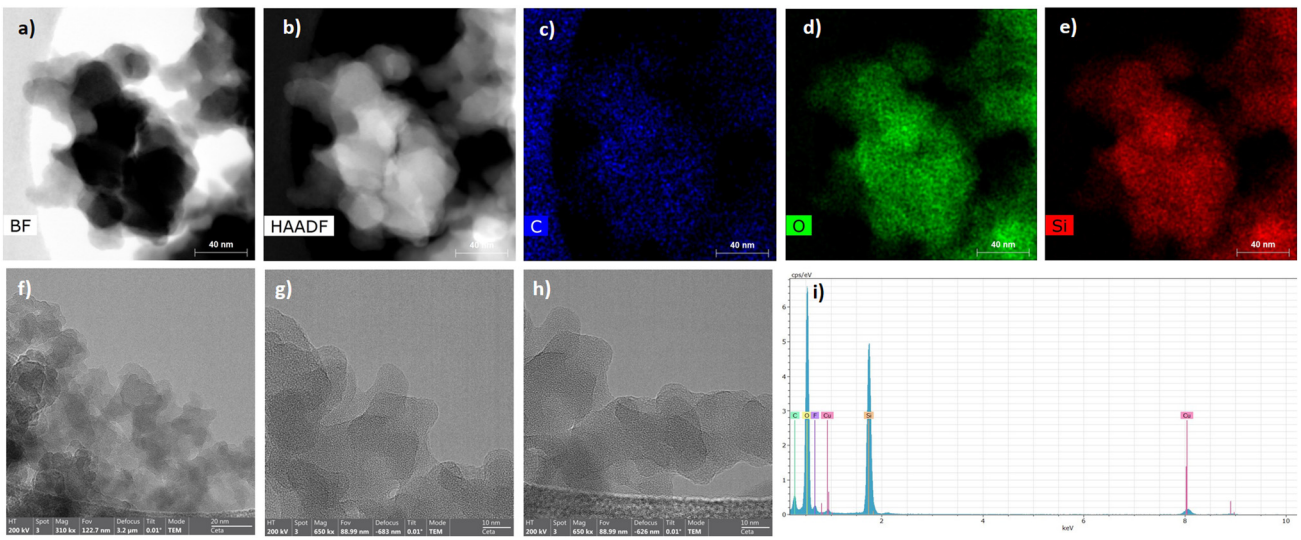

Fig. 2 (a and b) Structural and (c–e) elemental TEM images of the ACTD@SiO_2 nanoparticles. (f–h) High resolution TEM images and (i) elemental composition of the ACTD@SiO_2 nanoparticles.

strips before and after exposure to TATP vapors were measured using a Hamamatsu C10082CA mini-spectrometer, and the measurements are carried out in the same room immediately after exposure to TATP vapors. For excitation, a LED (Hamamatsu L14310-115)[33] with its power supply (Hamamatsu C14052-1-A3) and an optical fiber (Hamamatsu A15362-01) connected to a mini-spectrometer (Hamamatsu C10082CA mini-spectrometer)[34] were placed 7 cm away from a quartz cell where the glass sensing strips were introduced for measurement (Fig. 3). The intensity of the LED was regulated by a homemade shutter (circular black cardboard with a 3 mm central hole). All measurements were also

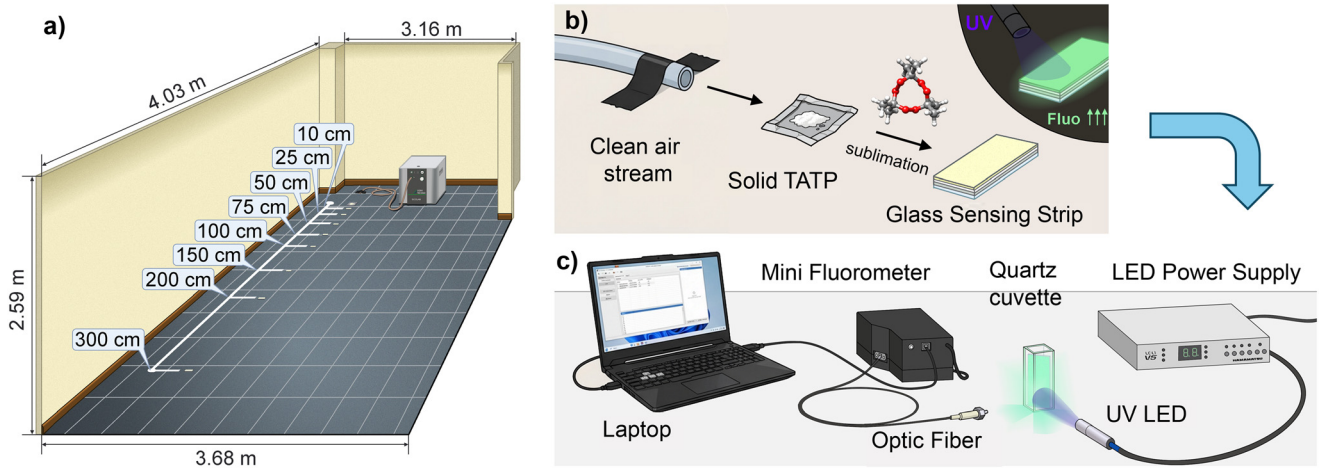

Fig. 3 (a) Measurements of the office where the experiments were performed, showing an image of the clean air compressor. (b) Detailed arrangement of the TATP sample in between the airflow and a sensing strip. Inset: a picture of the intrinsic fluorescence of a sensing strip. (c) Arrangement of the power supply, LED, fibre optics and mini-spectrometer for measurements of sensing strips.

repeated by using an Edinburgh FLS980 spectrometer. These measurements were used as a double check of the performance and reliability of the portable minifluorometer compared to a high-tech fluorometer.

Experiments were repeated on different days, and the results were checked by comparison of measurements from both spectrometers, concluding that measurements from both spectrometers were coherent, therefore, the reliability of the data from the Hamamatsu C10082CA mini-spectrometer was ensured (Fig. 4). For an easy visualization of the data, first we plotted the emission intensity variation before and after exposure to TATP vapours *versus* the distance to the TATP source, then, a common initial emission level was established by using the lowest value measured for the strips prior to the exposure to TATP vapours, finally, a subtraction was made between the final and initial emission, generating a graph of emission variation as a function of the distance to the TATP source plotted as a 3D representation of the information for both sets of measurements (Fig. 4). For comparison purposes, the mean and error of the variation of the fluorescence emission (%) as a function of the distance to the TATP source, measured by both fluorometers, was also plotted, showing similar tendencies in both series of measurements (Fig. 4).

From both plots it was clear that the tendency to detect the TATP vapor by fluorescence variations as the sensing material is closer to the source is maintained, therefore the sensing strips can operate under operational conditions where TATP vapour is present. From the standard amount of 5 mg TATP evaporated during the experiments (the room has

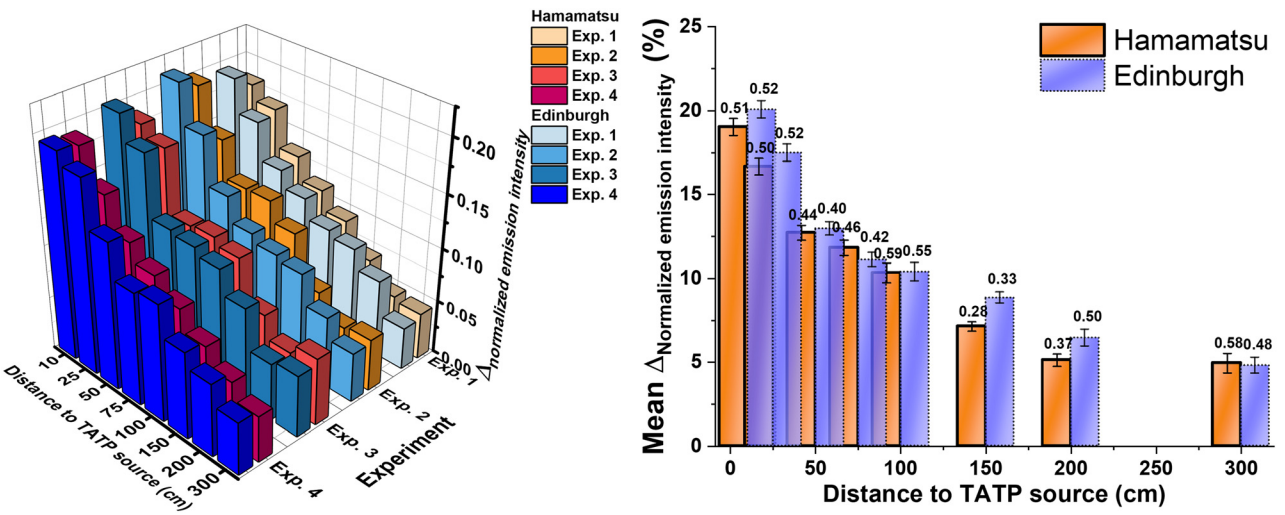

Fig. 4 (Left) 3D representation of the variation of the normalized emission intensity as a function of the distance to the TATP source measured using the Hamamatsu C10082CA mini-spectrometer (straw yellow to dark pink) and the Edinburgh FLS980 spectrometer (light blue to navy blue). (Right) Mean and error of the variation of the fluorescence emission (%) as a function of the distance to the TATP source, measured by the Hamamatsu C10082CA mini-spectrometer (orange) and by the Edinburgh FLS980 spectrometer (transparent purple), used for the validation of the previous measurements.

a volume of 40.7 m^3), a minimum concentration of 0.12 milligrams per cubic meter of air was the working limit of TATP measured at the farthest distance in the experiments. If we consider that a cubic meter of air weighs 1.2 kg, our working concentration limit is 10 ppb, which, considering such simple methodology, competes with currently known working detection limits[35–37] and with more sophisticated and expensive methods in terms of sensitivity and selectivity.[38,39]

The set of measurements by using the semi-autonomous mobile sensing platform and the sensing strips at fixed positions

Miniaturization of the system was performed by substituting the laptop with a mini-PC and a Wi-Fi communicated with a mobile phone (Oppo Find X3 Pro) and an Excel app for measurements (Fig. 5) (see the SI section, Videos S1–S5). We first checked that the measurements were comparable to the tabletop previous system and then inserted the new device system into a robotic mobile platform assembled in the laboratory, that included a custom-made box constructed by 3D impression, containing all electronics and a mobile cart guide for the sensing strip to perform measurements before and after the presence of airborne TATP (Fig. 5).

A series of detection experiments with the mobile platform were then performed (Fig. 6). Blank experiments for background measures were taken in all experiments (Fig. 6a). The measurements in the presence of TATP were performed by placing the TATP sample (experiments were standardized to 5 mg of TATP) on top of a height-adjustable laboratory stool (Fig. 6b) instead of on the floor, the air stream was maintained (100 cm^3 min^{-1}, 0.8 cm internal diameter), and the measurements were taken at similar distances from the vapor source as in previous cases, 10 to 200 cm away from the TATP source, at similar temperature and time for every measurement, 25 °C and 30 min. The mobile platform drew in outside air through a suction system, activated manually from the operator's control panel or automatically through the vehicle's internal programming, and the air was subsequently evacuated through the air outlet nozzles (100 cm^3 min^{-1} to maintain the continuous flow of clean air). An initial comparative analysis of the sensing strip deposited inside the robot on the sample cart, and the subsequent analysis once the outside air suction time has been concluded, was performed in all cases. The sample remained inside the analysis chamber for a programmed time, 2 min, and after that time, the sample carriage, along with the sensing strip, returned to its initial position, sliding on the guide base. The movement of the sample carriage was carried out by the action of a gearwheel, the rack of the sample carriage, and a motor housed on a support, controlled by its corresponding hardware and programming (Fig. S27–S29). Both the sample carriage and the sensing strip moved between two fixed points, therefore the analysis was always performed in the same position. For general use, once the analysis was complete, if it was positive, the vehicle emitted an alarm sound and displayed a red message on the mobile device. In contrast, when the analysis was negative, a green message was displayed. Communication between the robot and the mobile device located on the control station was carried out wirelessly *via* a modem housed in the communication support. The sample acquisition, sampling, and analysis system, comprising a guide base, sample carriage, gear wheel,

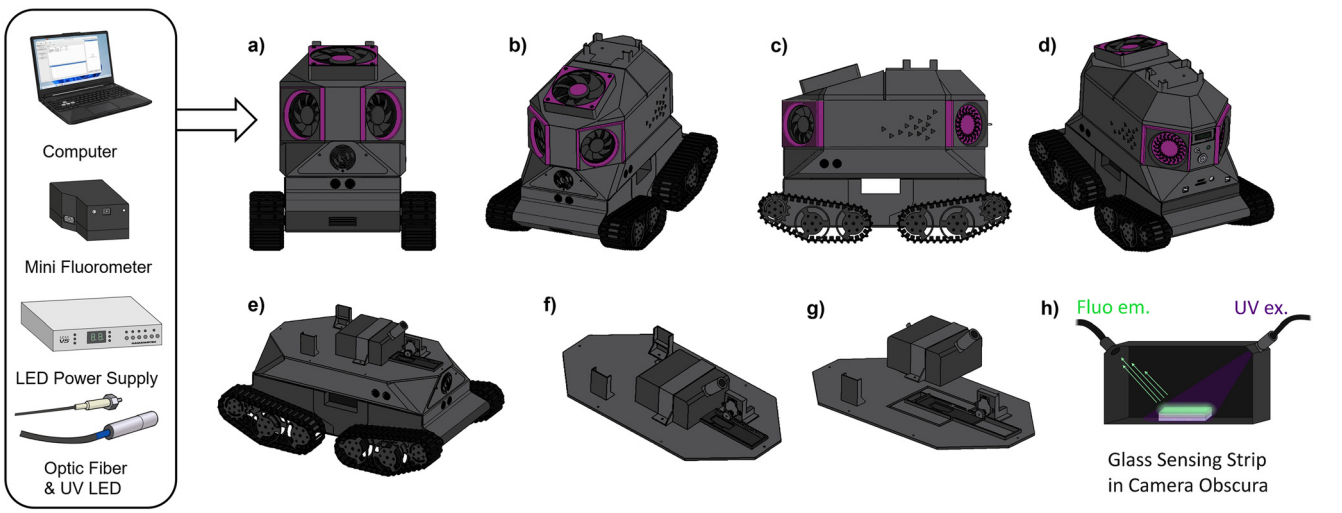

Fig. 5 Inset box on the left: the components of the miniaturized system used for the portable sensing device. (a) Front and (b) oblique front view of the mobile platform, (c) side view and (d) oblique rear view of the mobile platform with the box for electronics, portable fluorometer, LED (intensity at 2%), and mini-PC, (e) the mobile platform stripped of the box cover, showing the camera obscura and the mechanism for inserting the sensing strips, and (f and g) detailed view of the sensing strip insertion mechanism and the internal sensing strip cart guide. (h) Sensing strip between the LED and the fluorometer optic fibre for measurements of fluorescence differences before and after the presence of TATP, inside the dark chamber.

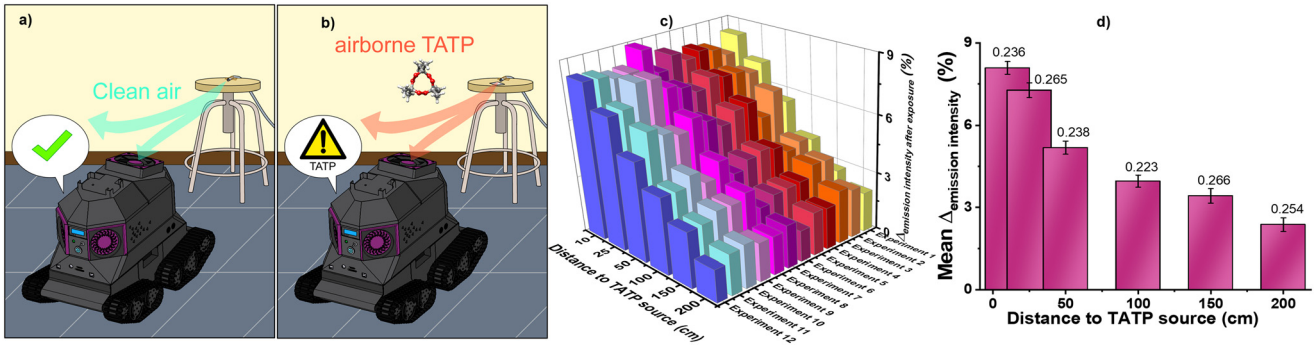

Fig. 6 (a) Blank test with no TATP. (b) Arrangement of the TATP sample for measurements with the mobile platform. (c) 3D bar graph representing the variation of the fluorescence emission of the mobile sensing platform (%) as a function of the distance to the TATP source in experiments 1–12. (d) Column + label graph representing the mean and error of the variation of the fluorescence emission measured by the mobile sensing platform (%) as a function of the distance to the TATP source.

motor support, an electric motor, cylindrical coupling, UV supports, and a guide base, along with the measuring devices (minifluorometer, UV light emitter) and data management device, were located within the upper fairing, which consisted of the upper sample cover, the upper cover for measuring devices, and the middle fairing. The vehicle was moved by a traction system composed of caterpillar wheels and electric motors. Both the middle fairing and the front fairing had mapping sensors that allowed the vehicle to be guided when in autonomous mode. The results of the experiments were then collected by an Excel app by the control system (Fig. 6).

From the results plotted in Fig. 6 it was clear that by carrying the traces of airborne TATP over the sensing strip, inside the sample chamber of the semiautonomous platform at the same air flow, the conditions previously optimized for the sensing strips were kept. Therefore, the relation between the enhancement of the fluorescence signal with the proximity of the TATP source was maintained (Fig. 6c and d), and the performance of the system was demonstrated as suitable for practical purposes under operational conditions.

Measurements by using the semi-autonomous mobile sensing platform and the sensing strips moving in the room

Additionally, a set of 5 experiments was carried out consisting of driving the robot inside the room containing TATP and causing the device to move around the entire room while passing at different distances from the TATP source for a period of 30 minutes. Fluorescence measurements of the sensing material were acquired before and after the mobile sensing platform, containing the sensing strips, was forced to move along the room in which the TATP was placed. For every one of the experiments, control measurements of the fluorescence of the sensing material in the mobile sensing platform were performed after following an identical route in the room lacking TATP (Fig. 7a).

Finally, variation of the fluorescence emission at the wavelength of maximum emission (525 nm) was calculated

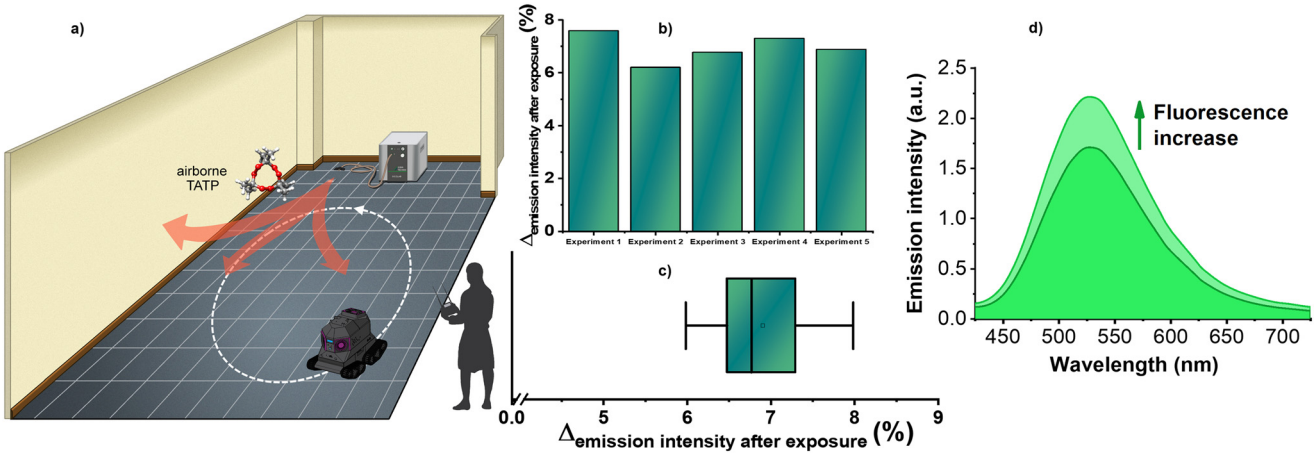

Fig. 7 (a) A cartoon of the experiment of the mobile sensing platform moving in the room. (b) 2D bar chart representing the variation (%) of the fluorescence emission of the mobile platform sensing material in experiments 1 to 5. (c) Box and whisker plot representing the variation (%) of the fluorescence emission of the mobile platform sensing material in experiments 1 to 5. (d) Fluorescence spectra showing an example of the variation increase of the fluorescence emission measured by using the mobile platform sensing material.

for every experiment. The emission of the sensing material increased by an average of 6.95 ± 0.66% over the 5 experiments, with a standard deviation of 0.53. The graphs shown in Fig. 7 were obtained as graphic representation of the variation of the fluorescence emission. From the results plotted in Fig. 7 it can be noticed that the fluctuations of the data were much higher than in cases where the passive air flow was used but the performance of the system is maintained, which made the system suitable for its use in operational scenarios, confined public spaces where TATP is subliming from a hidden source, as a contribution to the fight to terrorism in cases where IEDs containing TATP are used.

Experimental

A complete description of the general methods used in the experimental part, synthesis of the active dye, complete characterization of active dye, all experimental details, materials, devices and protocols is given in the SI section.

Conclusions

In conclusion, we have developed a new TATP sensing material by supporting a fluorogenic probe on silica, polydimethylsiloxane, and glass slides, to be used in a mechanized device for semi-autonomous measurements of airborne TATP. By using a UV LED and a commercial micro-fluorometer as the measuring block, a mini-PC and a Wi-Fi card as the control block, all integrated into a bespoke mobile platform, and a mobile phone as the receiver, we have constructed the first semiautonomous airborne TATP detector system that can be used for scanning IEDs in operational environments. It worked by exposing a sensing stick to the air flow in a room and sending the measurements to a mobile phone. The presence of TATP is subsequently detected by the difference in the fluorescence signal from the initial and final measurements. The system has been improved for application in confined public spaces of buildings where the threat of IEDs including TATP is suspected.

Author contributions

I. Abajo-Cuadrado carried out the fluorescence tests and wrote the experimental report on which the paper is based. A. Revilla-Cuesta performed the deposition of the composite material. R. Fernández-Ordóñez performed the assembly of the mechanical components and the 3D printing of the structural components of the robotic system. J. R. Santana-Tejada performed the communications protocols between the electronic components of the mobile sensing platform. C. Almeida-Estévez performed part of the synthesis of starting materials. Y. Moreno-Macías performed part of the synthesis of starting materials and crafted the drawings representing the room experiments. Hernando-Muñoz performed the characterization tests of the starting materials. J. García-Calvo performed the characterization spectra of the starting materials. M. Avella performed the TEM characterization of the sensing material. T. Torroba supervised the work and wrote the manuscript with the contributions of all authors.

Conflicts of interest

There are no conflicts to declare.

Data availability

The data supporting this article have been included as part of the supplementary information (SI).

Supplementary information: complete description of materials and devices, NMR, HRMS, UV and FL spectra, all data corresponding to airborne TATP detection experiments. See DOI: https://doi.org/10.1039/d5sd00218d.

Acknowledgements

This research was funded by the Ministerio de Ciencia, Innovación y Universidades of Spain (Grants PDC2022–133955-I00 and PID2022–142318NB-I00).

References

1 IED Attack, *Improvised Explosive Devices*, National Academies and the Department of Homeland Security, Dec. 15, 2020, https://www.dhs.gov/xlibrary/assets/prep_ied_fact_sheet.pdf, accessed 05/11/2025.
2 Europol, *European Union Terrorism Situation and Trend Report*, Publications Office of the European Union, Luxembourg, 2025, https://www.europol.europa.eu/cms/sites/default/files/documents/EU_TE-SAT_2025.pdf, accessed 05/11/2025.
3 L. Türker, Peroxide Based Organic Explosives, *Earthline J. Chem. Sci.*, 2021, **6**, 165–208, DOI: 10.34198/ejcs.6221.165208.
4 Brussels explosions: What we know about airport and metro attacks, https://www.bbc.com/news/world-europe-35869985, accessed 05/11/2025.
5 Expert Discusses Chemical That Prompts Carry-On Liquid Ban, https://www.aviationpros.com/home/news/10397744/expert-discusses-chemical-that-prompts-carry-on-liquid-ban, accessed 05/11/2025.
6 L. E. De Greeff, M. M. Cerreta and C. J. Katilie, Variation in the headspace of bulk hexamethylene triperoxide diamine (HMTD) with time, environment, and formulation, *Forensic Chem.*, 2017, **4**, 41–50, DOI: 10.1016/j.forc.2017.03.001.
7 A. Simon, L. Lazarowski, J. A. Barrow, K. Van Arsdale, M. Singletary, C. Angle, P. Waggoner, J. Wagner, K. Giles, T. Fischer, B. Rogers and W. MacCrehan, Validation of a polymer odor capture-and-release (POCR) aid for training canines to detect triacetone triperoxide (TATP), *Forensic Chem.*, 2022, **31**, 100454, DOI: 10.1016/j.forc.2022.100454.
8 TSA Expanding Explosive Trace Detection Measures at Airports Nationwide, https://ohsonline.com/articles/2010/02/

22/tsa-expanding-etd-measures.aspx?admgarea=news, accessed 05/11/2025.
9 Applicability of Portable Explosive Detection Devices in Transit Environments, TCRP Report 86, https://www.trb.org/publications/tcrp/tcrp_rpt_86v6.pdf, accessed 05/11/2025.
10 W. Wang, H. Li, W. Huang, C. Chen, C. Xu, H. Ruan, B. Li and H. Li, Recent development and trends in the detection of peroxide-based explosives, *Talanta*, 2023, **264**, 124763, DOI: 10.1016/j.talanta.2023.124763.
11 M. Brockmann, G. Glotz, J.-S. von Glasenapp, L. Unterriker, D. Neshchadin, G. Gescheidt and R. Herges, Highly Sensitive, Easy-to-Use, One-Step Detection of Peroxide-, Nitrate- and Chlorate-Based Explosives with Electron-Rich Ni Porphyrins, *J. Am. Chem. Soc.*, 2024, **146**, 13010–13024, DOI: 10.1021/jacs.3c14118.
12 A. Revilla-Cuesta, I. Abajo-Cuadrado, L. Quadrini, S. Failli, A. Rodríguez-Rubio, J. V. Cuevas, C. Hernando-Muñoz, J. García-Calvo and T. Torroba, Chemical speciation of methylmercury and mercury(II) cations in fish by new fluorogenic naphthalimide alkynyl gold complexes: The ultimate test for detecting fish contamination, *Sens. Actuators, B*, 2024, **421**, 136492, DOI: 10.1016/j.snb.2024.136492.
13 A. Revilla-Cuesta, I. Abajo-Cuadrado, M. Medrano, M. M. Salgado, G. Pecori, T. Rodríguez, C. Hernando-Muñoz, J. García-Calvo, J. Arcos and T. Torroba, New fluorescent reporters capable of Ultra-sensitively detecting trinitrotoluene on surfaces: A proof-of-concept for finding hidden nitroaromatics in the workroom, *J. Photochem. Photobiol., A*, 2023, **444**, 114911, DOI: 10.1016/j.jphotochem.2023.114911.
14 S. Lapcinska, A. Revilla-Cuesta, I. Abajo-Cuadrado, J. V. Cuevas, M. Avella, P. Arsenyan and T. Torroba, Dye-modified silica–anatase nanoparticles for the ultrasensitive fluorogenic detection of the improvised explosive TATP in an air microfluidic device, *Mater. Chem. Front.*, 2021, **5**, 8097–8107, DOI: 10.1039/D1QM01041G.
15 B. Díaz de Greñu, D. Moreno, T. Torroba, A. Berg, J. Gunnars, T. Nilsson, R. Nyman, M. Persson, J. Pettersson, I. Eklind and P. Wästerby, Fluorescent Discrimination between Traces of Chemical Warfare Agents and Their Mimics, *J. Am. Chem. Soc.*, 2014, **136**, 4125–4128, DOI: 10.1021/ja500710m.
16 P. M. Bulemo, D.-H. Kim, H. Shin, H.-J. Cho, W.-T. Koo, S.-J. Choi, Ch. Park, J. Ahn, A. T. Güntner, R. M. Penner and I.-D. Kim, Selectivity in Chemiresistive Gas Sensors: Strategies and Challenges, *Chem. Rev.*, 2025, **125**, 4111–4183, DOI: 10.1021/acs.chemrev.4c00592.
17 K. C. To, S. Ben-Jaber and I. P. Parkin, Recent Developments in the Field of Explosive Trace Detection, *ACS Nano*, 2020, **14**, 10804–10833, DOI: 10.1021/acsnano.0c01579.
18 L. Wang, J. Song and C. Yu, Recent progress on mass-sensitive gas sensors for environmental and industrial applications, *Measurement*, 2025, **249**, 117039, DOI: 10.1016/j.measurement.2025.117039.
19 P. Liu, X. Guo, C. Liang, B. Du, Y. Tan, H. Zheng, C. Min, Y. Guo and X. Yang, Rapid Detection of Trace Nitro-Explosives under UV Irradiation by Electronic Nose with Neural Networks, *ACS Appl. Mater. Interfaces*, 2023, **15**, 36539–36549, DOI: 10.1021/acsami.3c06498.
20 S. Khan, U. Valiyaneerilakkal, S. Kumar, A. Singh, A. Ahmed, H. C. S. Perera, R. Mahadeva, J. Alawatugoda and S. Arya, Nanosensors in hazardous explosives trace detection – challenges and Future directions, *Microchem. J.*, 2024, **200**, 110474, DOI: 10.1016/j.microc.2024.110474.
21 M. Amani, Y. Chu, K. L. Waterman, C. M. Hurley, M. J. Platek and O. J. Gregory, Detection of triacetone triperoxide (TATP) using a thermodynamic based gas sensor, *Sens. Actuators, B*, 2012, **162**, 7–13, DOI: 10.1016/j.snb.2011.11.019.
22 M. Warzecha, G. Morris, A. J. McLean, J. Calvo-Castro and C. J. McHugh, Detection of Nitroaromatic and Peroxide-Based Explosives with Amine- and Phosphine-Functionalized Diketopyrrolopyrroles, *ACS Appl. Mater. Interfaces*, 2023, **15**, 27915–27927, DOI: 10.1021/acsami.3c02714.
23 A. De Iacovo, F. Mitri, S. De Santis, C. Giansante and L. Colace, Colloidal Quantum Dots for Explosive Detection: Trends and Perspectives, *ACS Sens.*, 2024, **9**, 555–576, DOI: 10.1021/acssensors.3c02097.
24 R. Qiao, Y. Li, R. Zhu, H. Bai, C. Zhao, B. Zu and Z. Cai, Carbonized polymer dots for discrimination of 2,4,6-trinitrotoluene and 2,4,6-trinitrophenol, *J. Hazard. Mater.*, 2025, **491**, 137944, DOI: 10.1016/j.jhazmat.2025.137944.
25 M. A. Darwish, W. Abd-Elaziem, A. Elsheikh and A. A. Zayed, Advancements in nanomaterials for nanosensors: a comprehensive review, *Nanoscale Adv.*, 2024, **6**, 4015–4046, DOI: 10.1039/d4na00214h.
26 G. D. Crapper, A. S. M. Green, J. R. Dean and J. J. Perry, Investigation and analysis of explosive traces in public locations with no military context: a critical review, *Anal. Methods*, 2025, **17**, 3370–3380, DOI: 10.1039/d5ay00183h.
27 T. P. Forbes and E. Sisco, Recent advances in ambient mass spectrometry of trace explosives, *Analyst*, 2018, **143**, 1948–1969, DOI: 10.1039/c7an02066j.
28 K. Hasselmann, M. Malizia, R. Caballero, F. Polisano, S. Govindaraj, J. Stigler, O. Ilchenko, M. Bajic and G. De Cubber, A multi-robot system for the detection of explosive devices, *IEEE ICRA Workshop on Field Robotics*, 2024, DOI: 10.48550/ARXIV.2404.14167, accessed 05/11/2025.
29 X. Liu, X. Liu, B. Li, X. Zhang and B. Hu, Lab-on-Robot: Unmanned Mass Spectrometry Robot for Direct Sample Analysis in Hazardous and Radioactive Environments, *Anal. Chem.*, 2025, **97**, 9126–9130, DOI: 10.1021/acs.analchem.5c01237.
30 A. Sanluis-Verdes, P. Colomer-Vidal, F. Rodriguez-Ventura, M. Bello-Villarino, M. Spinola-Amilibia, E. Ruiz-Lopez, R. Illanes-Vicioso, P. Castroviejo, R. Aiese Cigliano, M. Montoya, P. Falabella, C. Pesquera, L. Gonzalez-Legarreta, E. Arias-Palomo, M. Solà, T. Torroba, C. F. Arias and F. Bertocchini, Wax worm saliva and the enzymes therein are the key to polyethylene degradation by Galleria mellonella, *Nat. Commun.*, 2022, **13**, 5568, DOI: 10.1038/s41467-022-33127-w.
31 M. Spínola-Amilibia, R. Illanes-Vicioso, E. Ruiz-López, P. Colomer-Vidal, F. Rodriguez-Ventura, R. Peces Pérez, C. F. Arias, T. Torroba, M. Solà, E. Arias-Palomo and F. Bertocchini, Plastic degradation by insect hexamerins: Near-

atomic resolution structures of the polyethylene-degrading proteins from the wax worm saliva, *Sci. Adv.*, 2023, **9**, eadi6813, DOI: 10.1126/sciadv.adi6813.

32 A. Revilla-Cuesta, I. Abajo-Cuadrado, M. Medrano, M. M. Salgado, M. Avella, M. T. Rodríguez, J. García-Calvo and T. Torroba, Silica Nanoparticle/Fluorescent Dye Assembly Capable of Ultrasensitively Detecting Airborne Triacetone Triperoxide: Proof-of-Concept Detection of Improvised Explosive Devices in the Workroom, *ACS Appl. Mater. Interfaces*, 2023, **15**, 32024–32036, DOI: 10.1021/acsami.3c05931.

33 https://www.hamamatsu.com/eu/en/product/light-and-radiation-sources/uv-led-light-source/uv-led-light-source_spot-irradiation/L14310_L14311.html, accessed 05/11/2025.

34 https://www.hamamatsu.com/eu/en/product/optical-sensors/spectrometers/mini-spectrometer/C10082CA.html, accessed 05/11/2025.

35 D. S. Viswanath, T. K. Ghosh and V. M. Boddu, *Emerging Energetic Materials: Synthesis, Physicochemical, and Detonation Properties*, Springer, Dordrecht, The Netherlands, 2018, ch. 10.4, pp. 276–279, DOI: 10.1007/978-94-024-1201-7.

36 T. Wasilewski and J. Gębicki, Emerging Strategies for Enhancing Detection of Explosives by Artificial Olfaction, *Microchem. J.*, 2021, **164**, 106025, DOI: 10.1016/j.microc.2021.106025.

37 A.-F. A. Mohammed, K. Y. Nabat, T. Jiang and L. Liu, Recent innovations in explosive trace detection: Advances and emerging technologies, *Trends Environ. Anal. Chem.*, 2025, **46**, e00261, DOI: 10.1016/j.teac.2025.e00261.

38 C. Schaefer, M. Lippmann, M. Beukers, N. Beijer, B. van de Kamp, J. Knotter and S. Zimmermann, Detection of Triacetone Triperoxide by High Kinetic Energy Ion Mobility Spectrometry, *Anal. Chem.*, 2023, **95**, 17099–17107, DOI: 10.1021/acs.analchem.3c04101.

39 I. A. Buryakova and T. I. Buryakov, State-of-the-Art Technologies in Explosives Detection, *J. Anal. Chem.*, 2025, **80**, 591–607, DOI: 10.1134/S1061934825700029.